Received: 30 October 2019 | Revised: 2 January 2020 | Accepted: 6 February 2020

DOI: 10.1111/jace.17061

Journal of the American Ceramic Society

ORIGINAL ARTICLE

Structural and thermal behavior of 45S5 Bioglass®-based compositions containing alumina and strontium

Mariana S. Araujo[1] | **Antonio C. Silva**[1] | **José F. Bartolomé**[2] | **Sonia Mello-Castanho**[1]

[1]Department of Materials Science and Technology, Instituto de Pesquisas Energéticas e Nucleares, São Paulo, SP, Brazil

[2]Instituto de Ciencia de Materiales de Madrid (ICMM), Consejo Superior de Investigaciones Científicas (CSIC), Madrid, Spain

Correspondence
José F. Bartolomé, Instituto de Ciencia de Materiales de Madrid (ICMM), Consejo Superior de Investigaciones Científicas (CSIC), Madrid, Spain.
Email: jbartolo@icmm.csic.es

Funding information
Coordenação de Aperfeiçoamento de Pessoal de Nível Superior, Grant/Award Number: 88881.189953/2018-01; Conselho Nacional de Desenvolvimento Científico e Tecnológico, Grant/Award Number: 142172/2016-2; Fundação de Amparo à Pesquisa do Estado de São Paulo, Grant/Award Number: 2000/02483-9

Abstract

The present research exposes the influence of 2 mol% of Al_2O_3 and 2 mol% SrO in 45S5 Bioglass®-based compositions. Four compositions were produced to elucidate the difference in how both oxides influence structure and thermal behavior separately and their synergy when together. Thermal properties, crystallization tendency, and sintering behavior was evaluated by differential scanning calorimetry, hot stage microscopy, and dilatometry. Changes of medium-range structures were characterized by Q^n distribution of Raman spectroscopy and evaluation of ^{31}P, ^{27}Al, ^{23}Na, and ^{29}Si environment obtained by magic angle spinning nuclear magnetic resonance. Despite Q^n distribution was predominantly Q^2 in all samples, the composition criteria used enabled improved processing and stabilibity characteristics. The addition of Al_2O_3 and SrO promoted larger sinterability parameter (S_c) which indicates better sintering behavior, the glass stability against crystallization doubled (K_H) compared to 45S5 and the processing window enlarged from 106 to 171.

KEYWORDS

alumina, bioactive glasses, glass structure, strontium oxide, thermal properties

1 | INTRODUCTION

Bioactive glasses are in a general way compositions made from the Na_2O-CaO-SiO_2-P_2O_5 system and in some cases, associated with other metal oxides, but are characterized by forming a strong mechanical bond with the bone. The first bioactive glass was developed by Prof. Larry Hench in 1969 and has been widely used since the 80s because of its high biocompatibility. However, due to its high crystallization tendency and consequently limitation in applications that require heat treatments, many other glasses with distinct compositions has been also largely investigated.[1–4]

Glasses as a versatile material accept a large range of distinct cations in its structure and can be easily modified. However, the complexity in designing brand-new compositions as Bioglass® 45S5 is mainly due to the fact that a number of components involved results in being more difficult to control the relationship between composition, structure, and bioactivity.[5] Also, the properties of bioactive compositions reflect their ability to release a critical amount of carbonate apatite precursors ions in the surrounding host tissue to stimulate cellular processes.[6] Since these properties and processes of interaction are directly related to the glass network connectivity,[7,8] which can be evaluated by Q^n distribution, that is, concentration of bridging oxygens (BOs) per silicon tetrahedron that determines random glass arrangement.

Among many new models and compositions proposed during the past decades, the ion substitution in 45S5 composition was highlighted. The idea of incorporating therapeutically active ions such as strontium and/or aluminum can contribute to a material

with additional beneficial effects by providing tissue regeneration capabilities, enhanced bioactivity, and extended working range.[9,10] Strontium-containing bioactive glasses have already been recognized to affect bone growth in appropriate quantities.[11–14] Strontium itself has been used for osteoporosis prevention as a ranelate form (Protelos®).[15] The strontium addition in bioactive glasses combines the known regenerative properties of bioactive glasses with anabolic and anti-catabolic effects of strontium ions. Alumina addition in contrast, in quantities above 3 mol% can inhibit or diminish the interaction between material and host, however, its addition in small (up to 2 mol%) quantities can enhance bioactivity, mechanical, and thermal properties.[16,17]

Considering the modification of glass compositions, the careful design is the key factor to result in a suitable material for medical applications. The 45S5 Bioglass® was calculated near an eutectic point in the ternary soda lime silicate diagram due to its low melting temperature and as a composition with a high content of alkali cations is prone to percolate into channels and to exhibit mixed alkali effect even with small changes in network connectivity.

Based on this effect and the responsive equilibria of 45S5, the substitution of 2 mol% of silicon by alumina was proposed. That is because, usually alumina at low concentrations is associated with the silicate network as AlO_6 octahedra playing the role of stabilizer oxide, such as SrO. However, when alumina is present as AlO_4 tetrahedra, it will be at the SiO_4 tetrahedral network acting as a former oxide. The advantage of AlO_4 in the network is that it improves physicomechanical properties despite amplifying the processing window and increasing bioactivity. It is difficult to obtain AlO_4 units in a complex system because at concentrations lower than <5 mol% secondary formers ions (such as alumina) interact with the glass network in a way similar to alkali metals and alkaline earth metals,[18] that is, at low concentrations the R_xO_y acts as a network modifier. Substituting alumina in silicon percent is expected that the lack of the former oxide and for network maintenance the alumina will replace the silicon tetrahedral and incorporate into the network as AlO_4 units. Nevertheless, this will impact phosphorous subnetwork as calcium will be required to charge-balance AlO_4 units. Then, an addition of 2 mol% of strontium was considered to contribute to the enrichment of phosphorous environment and possibly provide stronger bonding among fragments of silicon network compensating feasible weakening of its network by the presence of alumina. Strontium oxide acts as a modifier oxide and is known to improve bone growth and regeneration while maintaining the general chemical and physical behavior of the base glass composition.[19]

Hence, to study substituted bioactive glasses compositions is still relevant to better understand how a strict chemical composition design can open a new way to functionalize structures of the bioactive glasses. Therefore the aim of this study is to elucidate the influence of low content of strontium oxide and alumina in four 45S5-based compositions, and consequently how they affect the glass structure and crystallization separately and their synergy when together. Also, the interaction between Al^{3+} and Sr^{2+} upon Bioglass-based compositions found in this study overcomes expectations reducing drawbacks of processing such as working window and empowering its use in applications that requires a thermal treatment.

2 | EXPERIMENTAL PROCEDURES

Four glass compositions containing Al_2O_3 and SrO were calculated in a molar base as presented in Table 1. For a more comprehensive study of the role of each oxide was considered samples containing them separately and together. Also, a sample of Bioglass® 45S5 (BioH) composition was made for comparative purposes.

The glasses were prepared from reagent-grade SiO_2 (99.0 wt%), CaO (99.0 wt%), Na_2CO_3 (95.0 wt%), Al_2O_3 (99.0 wt%), $Ca(H_2PO_4)\cdot 2H_2O$ (99.0%) and $Sr(NO_3)_2$ (99.0 wt%). Batches of 30 g were obtained by homogenizing the raw materials in an agate mortar for 10 minutes and subsequently melting it into a Pt-5%Au crucible at 1500°C for 1 hour in a vertical electric furnace. The glass samples were cast into bar molds (30 × 10 × 10) mm, annealed at 470°C for 2 hour and slowly cooled down to room temperature to remove thermal strain. The bulk samples were reserved, and a part of it was crushed and the particle size was reduced using an agate milling ball and then sieved to a size below 50 μm. The amorphous state of the samples was confirmed by powder X-ray diffraction (XRD; Bruker D8 ADVANCE); using CuKα radiation with 2θ from 10° to 70° and in steps of 0.1°/s.

In order to verify the crystalline phases in the studied compositions, the powders were axially pressed into discs and then, a heat treatment was carried out in a tubular furnace at 800°C for 2 hours under ambient atmosphere above a platinum plate.

TABLE 1 Nominal and measured (in parentheses) composition in mol%

Sample	SiO_2	P_2O_5	Na_2O	CaO	Al_2O_3	SrO
BioH(45S5)	46.1 (47.3)	2.6 (2.7)	24.4 (23.5)	26.9 (26.5)	—	—
BioAl	44.1 (46.5)	2.6 (3.3)	24.4 (21.0)	26.9 (26.8)	2.0 (2.4)	—
BioSr	45.2 (46.0)	2.5 (2.4)	23.9 (23.1)	26.4 (26.5)	—	2.0 (2.0)
BioAlSr	43.2 (43.7)	2.5 (2.3)	23.9 (23.3)	26,4 (26.2)	2.0 (2.3)	2.0 (2.2)

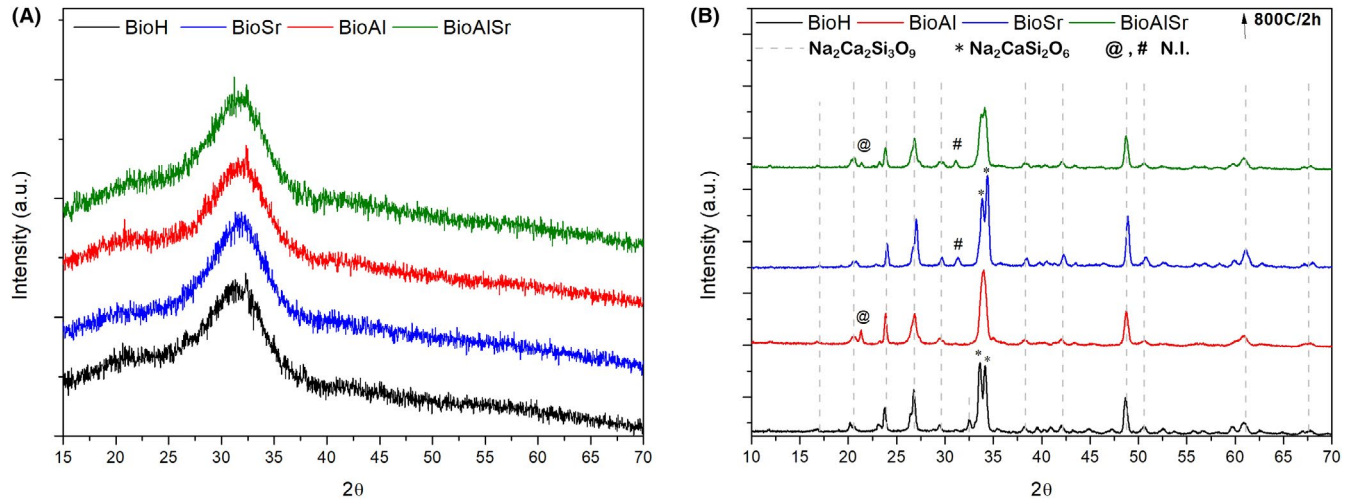

FIGURE 1 Diffractograms of samples BioH, BioSr, BioAl, and BioAlSr (A) as obtained and (B) heat treated at 800°C for 2 h [Color figure can be viewed at wileyonlinelibrary.com]

Phase identification of heat-treated samples was carried out by comparing XRD pattern obtained in the same conditions mentioned above with the standard JCPDS files.

The thermal behavior of the obtained samples was investigated by DSC (Netzsch, DSC 404F3 PEGASUS) recorded at a constant heating rate of 10 K·min^{-1} up to 800°C to obtain glass transition (T_g) and onset crystallization temperatures (T_x). Dilatometry (Bähr Thermoanalyse DIL 802) was conducted by the heating rate 5 K·min^{-1} to obtain T_g and thermal expansion coefficient (TEC) determined at 500°C using the dilatometry curves in the temperature range between 100°C and 500°C.

A side-view hot-stage microscope (HSM; EM 201) equipped with image analysis system and electrical furnace 1750/15 Leica was also used to obtain liquidus temperature and characteristic viscosity points (first shrinkage T_{FS}, maximum shrinkage T_M and flow T_l). The measurements were conducted in air with a heating rate of 10 K min^{-1}. The samples, cylinder-shaped and placed on an alumina support, were prepared with cold-pressed glass powder. The temperature was measured with a Pt/Rh (6/30) thermocouple contacted under the alumina support.

Fourier transform infrared spectroscopy (FTIR, Bruker IFS 66 VS) was performed by using a diffuse reflectance attachment within a range of 400-4000 cm^{-1} and a resolution of 2 cm^{-1}. The analysis provided an outlook of the evolution of the network connectivity according to changes in composition and also, after the crystallization heat treatment.

Magic angle spinning nuclear magnetic resonance (MAS-NMR; Bruker Advance 400) experiments were performed at room temperature for ^{29}Si (79.48 MHz) and ^{27}Al (104.26 MHz). ^{31}P (161.98 MHz) and ^{23}Na (105.80 MHz). Glass powders were packed into zirconia rotors. The samples were spun at 10 kHz, the number of scans 120 with a recycle delay time set to 10 seconds to minimize saturation effects. Estimated errors for chemical shifts and relative area are 0.2 ppm and 2% respectively. The analysis of ^{29}Si NRM spectra was carried out with the Fityk software assuming Gaussian peak profile. From the fitting of experimental envelopes, relative intensities of different components were deduced.

Raman spectroscopy was analyzed, using a micro-Raman spectrometer (WITEC, Confocal Raman Microscope Alpha300 R). The samples were excited by the 532 nm line of an Ar^+ laser and recorded with microscope objective 50x/0.7 at 60 seconds integration time with 45 mW power. The frequencies and the number of Raman bands reported in this study were obtained by considering Q species and vibrational groups contained in the kind of glasses and assuming Gaussian peak profile.

3 | RESULTS AND DISCUSSION

3.1 | Glass compostions and phase formation

In view that 45S5 belongs to the system SiO_2:CaO:Na_2O:P_2O_5 of which typical composition is given by 45.0SiO_2:24.5Na_2O:24.5CaO:6.0P_2O_5 (in wt%), this research was conducted by modifying it through the charge-balance destabilization of the vitreous network by previous addition of alumina and further, SrO in excess.

At 45S5, one-third of the silicon tetrahedron atoms corresponds to BOs. Its structure is the dominating chain-like (most Q_{Si}^2 units) occasionally attracted to each other by calcium (Ca^{2+}) ions. The role of calcium in these compositions is very important because its mobility dictates the ion exchange when in contact with an aqueous media.[20–22] So, it is directly connected to bioactivity. Either calcium, strontium

or sodium ions have more affinity to bond with phosphorous than silicon. Also, by field strength, the preference of NBOs will be Ca > Sr > Na. Recent studies already stated that there is no sign of Si-O-P bonds in 45S5, confirming the phase separations in this composition. Assuming the presence of phosphorous only as orthophosphate (PO_4^{3-}), its charge will be compensated by Ca^{2+} and Na^{+} will be rich.[23]

Compositions, as calculated and obtained determined by X-ray fluorescence chemical analysis, are presented in Table 1 expressed in mol%. The samples obtained were homogeneous and XRD confirmed their amorphous state (Figure 1A). However, all samples showed a broad shoulder in smaller 2θ angles, indicating an overlap of halos. This particularity has already been reported by other authors[24,25] in 45S5 and similar bioactive glasses that contain more than one alkali metals and can be an indication of the glass-in-glass phase separation of the material, ie, the segregation of two molten liquids before critical cooling. This is because each oxide plays a role in the glass structure formation acting as former, intermediaries or modifiers. The 45S5 composition although belonging to a system that contains silicon and phosphorus oxide both primary former only silicon oxide act like a former while phosphorous as orthophosphate (PO_4^{3-}) commonly segregates into clusters or subphase associated with Ca^{2+}.[18]

The study of the effect of heat treatment of bioactive glasses and the nature of the phase produced is important because it is required for several technical applications besides helping explore changes in arrangement e tendency of phase formations as compositions are modified. In order to investigate the crystalline phases in the present compositions the heat treatment was taken in higher temperature—at 800°C for 2 hours—that is, by this temperature considering the existence of two different phases—one rich in silicon and the other rich in phosphorous—both corresponding crystalline phases will be already developed.[26] The analysis of the XRD patterns after heat treatment is presented in Figure 1B. All spectra showed the presence of sodium-calcium-silicate—which is supposed to be the main crystalline phase.[27] Although the known difficulty in identifying the exact sodium-calcium-silicates phases as they exhibit very similar reference patterns, 45S5-like compositions belong to the combeite precipitation field. Still, Lefebvre et al[28] reported that structural transformations during heat treatment should be noted. Considering both SearchMatch database and references, the best fitting for all glass spectra was the patterns of combeite ($Na_2Ca_2Si_3O_9$; JCPDS 22-1455). However, taking into account peaks at 23.8°, 33.8° and 34° (2θ), a significant difference was noticed. For BioH and BioSr the peak at 23.8° was more intense and the peak at 34.1° (exhibited in BioAl and BioAlSr) was decomposed into two at 33.8° and 34.1° (*), these patterns are usually attributed to high combeite ($Na_2CaSi_2O_6$; JCPDS 77-2189) known to be isostructural to combeite itself. In general, high combeite is formed in higher temperatures (>900°C), however small changes in P_2O_5/NaO or prolonged heat treatment can accelerate its formation. The earlier formation of high combeite and other peaks less intense between 50° and 60° in BioH and BioSr could indicate a higher tendency to crystallization in comparison with BioAl and BioAlSr. Despite it non identified peaks placed on 21.4° (@) for alumina-containing glasses (BioAl and BioAlSr) and on 31.1° (#) for strontium-containing glasses (BioSr and BioAlSr) was observed. No phosphate-rich or strontium-containing phase was observed which is probably because they were below detectable levels.

The FT-IR spectra of untreated and crystallized glass powders are shown in Figure 2; The spectra of untreated samples exhibited three broad bands in the region of 400-1400 cm^{-1}. This lack of specific features is indicative of the

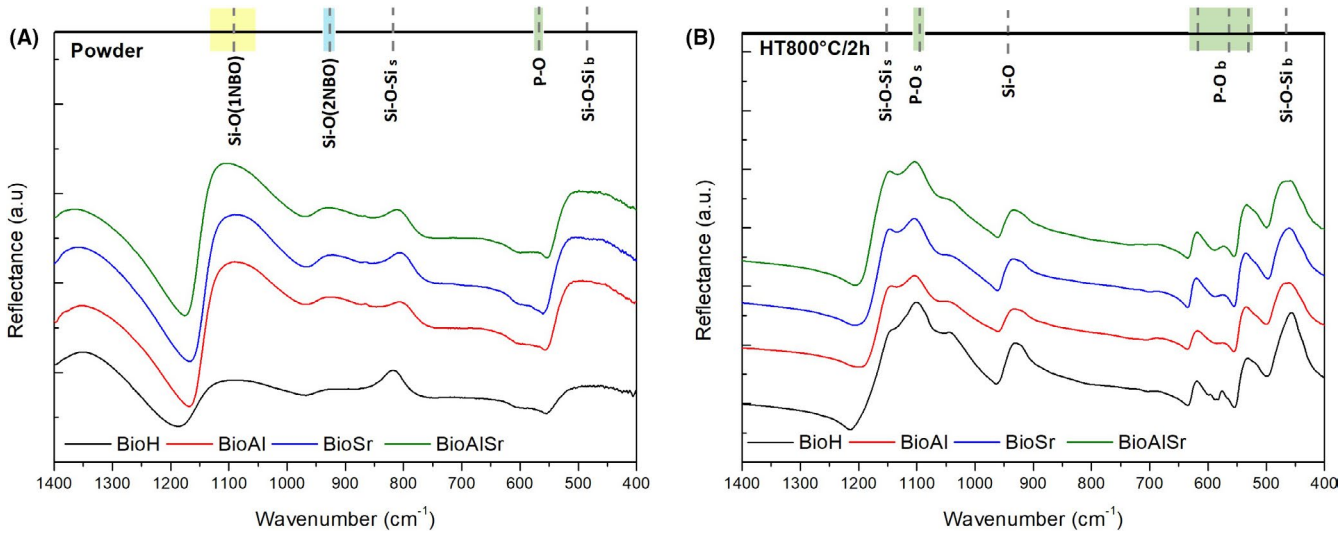

FIGURE 2 FTIR spectra of (A) untreated powder samples and (B) after crystallization treatment at 800°C for 2 h. FTIR, Fourier transform infrared spectroscopy [Color figure can be viewed at wileyonlinelibrary.com]

disorder of silicate and phosphate networks, and especially of the wide distribution of Q^n units in these glasses.[18,20] The most intense bands are in the region of 800-1300 cm^{-1} and correspond to the stretching vibrations of the silica tetrahedron with a different number of BOs or NBOs. And in all glasses, this region is divided into two transmission bands, one at 940 cm^{-1} assigned to the structure Q^2 (Si-O(2NBO)) and a second band in the range of 1000-1100 cm^{-1}, Si-O-Si always associated with Q^3 units. The third is the band less intense at 490 cm^{-1} assigned to Si-O-Si (bend). Peak development at 830 cm^{-1}, present in all samples, can be assigned to Si-O-Si s vibration between two neighboring SiO_4 tetrahedra.[29,30] A minor peak at 560 cm^{-1} attributed to amorphous P-O bend, in general, increases as crystallization occurs. The spectra of crystallized samples which were heat treated presented significant changes where the original broad bands are decomposed into several peaks and a new peak at 575 cm^{-1} emerges that could be related to the new crystalline phase. These changes are also highly connected to phosphorous content and occurrence in the glass network since vibrational modes of P linkages are mostly in the region between 472 and 602 cm^{-1}.[29]

3.2 | Glass transition temperature and sintering behavior

In order to evaluate the work temperatures and events that could affect the properties of the material after preparation, we were performed DSC analysis (Figure 3), dilatometry, and hot stage microscopy. From the obtained data, based on their thermal events, it was possible to determine the temperatures of glass transition (T_g), onset crystallization (T_x) and liquidus (T_l), and TEC at 500°C ($\alpha_{500°C}$). All the determinate temperatures are given in Table 2 as well as stability parameters such as processing window ($\Delta T = T_x - T_g$), glass stability against crystallization (K_H) and sinterability (S_c).[31,32] Considering the presence of two subnetwork and so two T_g, from the DSC curves was possible to observe that all samples did not present substantial changes in T_g—corresponded to the silicate phase (majority phase due to its concentration)—occurring between 520°C (BioH) and 539°C (BioSr). In contrast, a significant displacement of the crystallization peak was observed in samples containing alumina (BioAl and BioAlSr) besides evidencing the presence of a second T_{g2}—event already observed in bioactive glasses containing

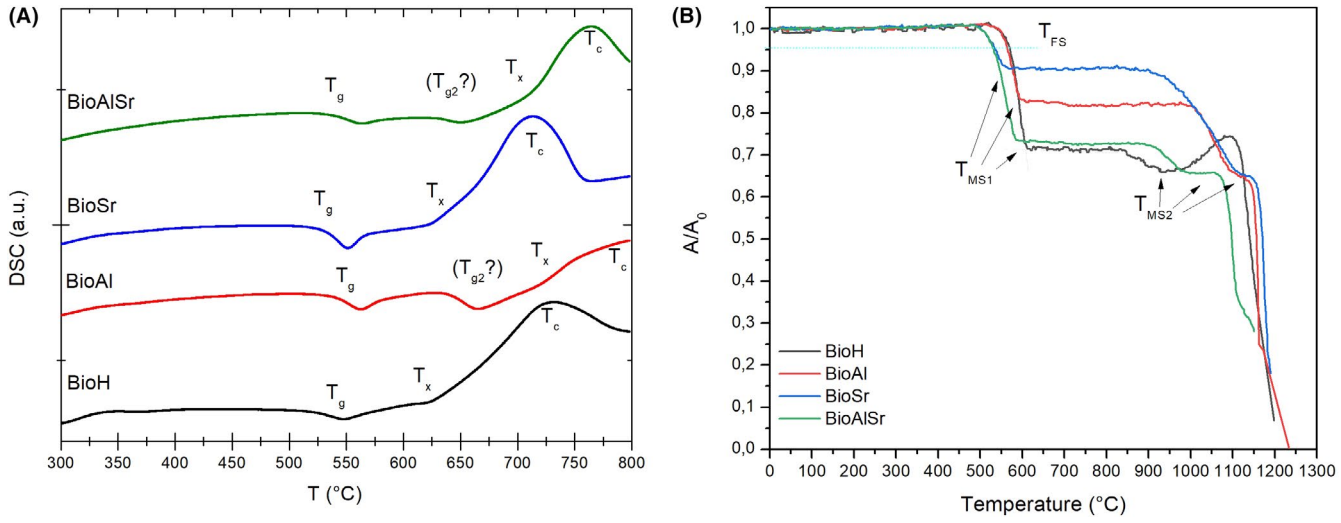

FIGURE 3 A, DSC curves of powder samples BioH, BioSr, BioAl, and BioAlSr up to 800°C. B, Glass compositions area variations (A/A0) from HSM as function of temperature. TFS, temperature of first shrinkage; TMS, temperature of maximum shrinkage [Color figure can be viewed at wileyonlinelibrary.com]

TABLE 2 Glass properties: temperatures (°C) of glass transition (T_g), onset of crystallization (T_x) obtained from DSC curves, first shrinkage (T_{FS}), maximum shrinkage (T_{MS1}; T_{MS2}), and liquidus (T_l). Parameters of glass stability S_c, ΔT and K_H(°C) and thermal expansion coefficient at 500°C ($\alpha_{500°C}$)

Tecnique	DSC (±2°C)		HSM (±5°C)				Parameters			Dilatometry
Sample	T_g	T_x	T_{FS}	T_{MS1}	T_{MS2}	T_l	S_c	ΔT	K_H	$\alpha_{500°C}$
BioH	520	626	569	609	927	1198	17	106	0.19	14.89×10^{-6}
BioAl	528	720	564	593	1089	1233	127	192	0.37	16.90×10^{-6}
BioSr	539	621	534	557	1110	1140	64	82	0.16	15.64×10^{-6}
BioAlSr	530	701	529	588	987	1151	113	171	0.38	15.69×10^{-6}

more than one alkali[8,33–35]—suggesting the impact of both alumina and strontium mostly in the orthophosphate subnetwork. The TEC obtained at 500°C from dilatometry varied from 14.89×10^{-6} (BioH) to 16.90×10^{-6} (BioAl) and were very similar for BioSr and BioAlSr corresponding to 15.64 and 15.69×10^{-6} respectively. Both alumina and strontium oxide presence caused an increase in TEC. By far the effect of strontium addition in TEC of bioactive glasses was not investigated. In general, the presence of alumina in glasses affects the thermal expansion causing a decrease in TEC due to its octahedral (AlO_6) coordination in the structure. However, we have noticed an increase of TEC in BioAl that could be because of the change in coordination in this composition, suggesting the presence of tetrahedral alumina (AlO_4)-generating covalent bonds with silicon which can cause an expansion of the network.[9,36] For all samples, TEC obtained was close to BioH and so adequate for biotechnical applications such as coatings.

The sintering behavior of the glass was studied by investigating fine-grained powder using HSM. Figure 4A shows that the sintering curves given to area variation (A/A_0) as a function of temperature for all glasses. The sintering temperature (T_{FS}) indicated in the image is defined by DIN51730 as the shrinkage of the initial sample height to 95%. The T_{MS} is the starting temperature of the plateau of constant sample height after the first shrinkage. Apparently, the addition of strontium has caused a decrease in T_{FS}. The samples exhibited two-stage sintering behavior implicating the presence of two $T_{MS.}$ The conclusion of first shrinkage stage is identified as T_{MS1} while of the second is T_{MS2}. For all glasses, the T_{MS1} was lower than crystallization temperature onset ($T_{MS1} < T_x$) meaning sintering precedes crystallization and so appears as an independent process. Still, a great difference in shrinkage was noticed, indicating different compacting behavior. Whereas BioH and BioAlSr contract ~30% of the area at the $T_{MS1,}$ BioAl shrinkage was about ~20% and BioSr only ~10%. Nevertheless, at $T_{MS2,}$ all samples presented a similar reduction in area about 35% resulting in good densification.

From temperatures obtained by both DSC curves and HSM (considering T_{MS1} as the predominant phase in all compositions) is possible to measure the glass stability against crystallization in two ways. One by the parameter proposed by Hruby, K_H which depends on temperatures of onset crystallization (T_x), glass transition temperature (T_g), and flow/liquidus temperature (T_l) where larger the parameter calculated greater the stability against crystallization on heating. On the other hand by the sinterability parameter (S_c) proposed by Lara et al[31] which is given by $T_x - T_{MS}$ and estimates the competition between sintering and crystallization where the greater the difference the more independent is the kinetics of both processes.[37] These two parameters must also be in accordance with ΔT, known as the process window and given by $T_x - T_g$. Glass BioH already recognized for its poor processing window and high tendency to crystallization presented the smaller values of both parameters indicating how associated are the kinetics of sintering and crystallization. BioSr, as well as BioH, presented high dependency only with a larger ΔT. Otherwise, both glasses containing alumina, BioAl and BioAlSr presented larger S_c which indicates better sintering/crystallization behavior and twice K_H compared to BioH and the amplified processing window.

3.3 | The structure of the glasses

The bioactive glasses are usually formed by open silicate network that is, interconnected in a combination of Q_{Si}^2 (chains and rings) and with a lower incidence of other Q^3_{Si} species. In respect of glass network arrangement, both P^{5+} and Si^{4+} tend to occur in tetrahedral coordination in oxide glasses. However, when the two elements are present in suchlike 45S5 compositions and for bioactive purposes, silicon will always act as network-former dictating the network-polymerization and phosphorous predominantly as orthophosphate ions cooperating to ensure the ionic mobility in aqueous medium by an accessible structure.[38–41] Figure 4 shows ^{29}Si MAS-NMR spectra and Table 3 specifies the deconvolution components and their percentages calculated from fractional areas. The spectra comprise four contributions: some residual Q_{Si}^1 and Q_{Si}^4 groups at −70 and −96 ppm, respectively, Q_{Si}^2 at −80 ppm and Q_{Si}^3 at −88 ppm. Even though all samples presented a similar spectrum and a chemical shift centered near −80 ppm indicating that Q_{Si}^2 units dominate the distributions, the center moved toward a higher resonance frequency. As a result, excluding BioH, all modified samples presented a gain in Q_{Si}^3 units in function of Q_{Si}^2. For instance, the fractional area of Q_{Si}^3 changed from 56 for BioH to 77% for BioAlSr.

Figure 5A shows the ^{31}P MAS-NMR chemical shift for the glasses. All spectra obtained are in the range of orthophosphate environment (PO_4^{3-}) known for charge-balance with a mixture of modifier cations. The spectra are centered at ≈8 ppm and located in the region between sodium (16 ppm) and calcium (3 ppm) orthophosphate. This reinforces that phosphorous in the extent compositions did not enter the glass network acting as a former oxide and so is not associated either with silicon or aluminum (in case of BioAl and BioAlSr). Also, the presence of alumina in 2 mol% did not affect the required charge compensation of orthophosphate species. Furthermore, comparing the samples with BioH, it can be noticed that their center presented a slight displacement toward higher ppm values, that is, sodium orthophosphate environment. That throw could suggest a greater contribution of Q_{Si}^2 structure.[38,42] The ^{29}Si MAS-NMR chemical shift previously discussed evidence of this suggestion.

Figure 5B shows ^{23}Na MAS-NMR spectra of the glasses. BioH, BioAl, and BioAlSr spectra were similar displaying

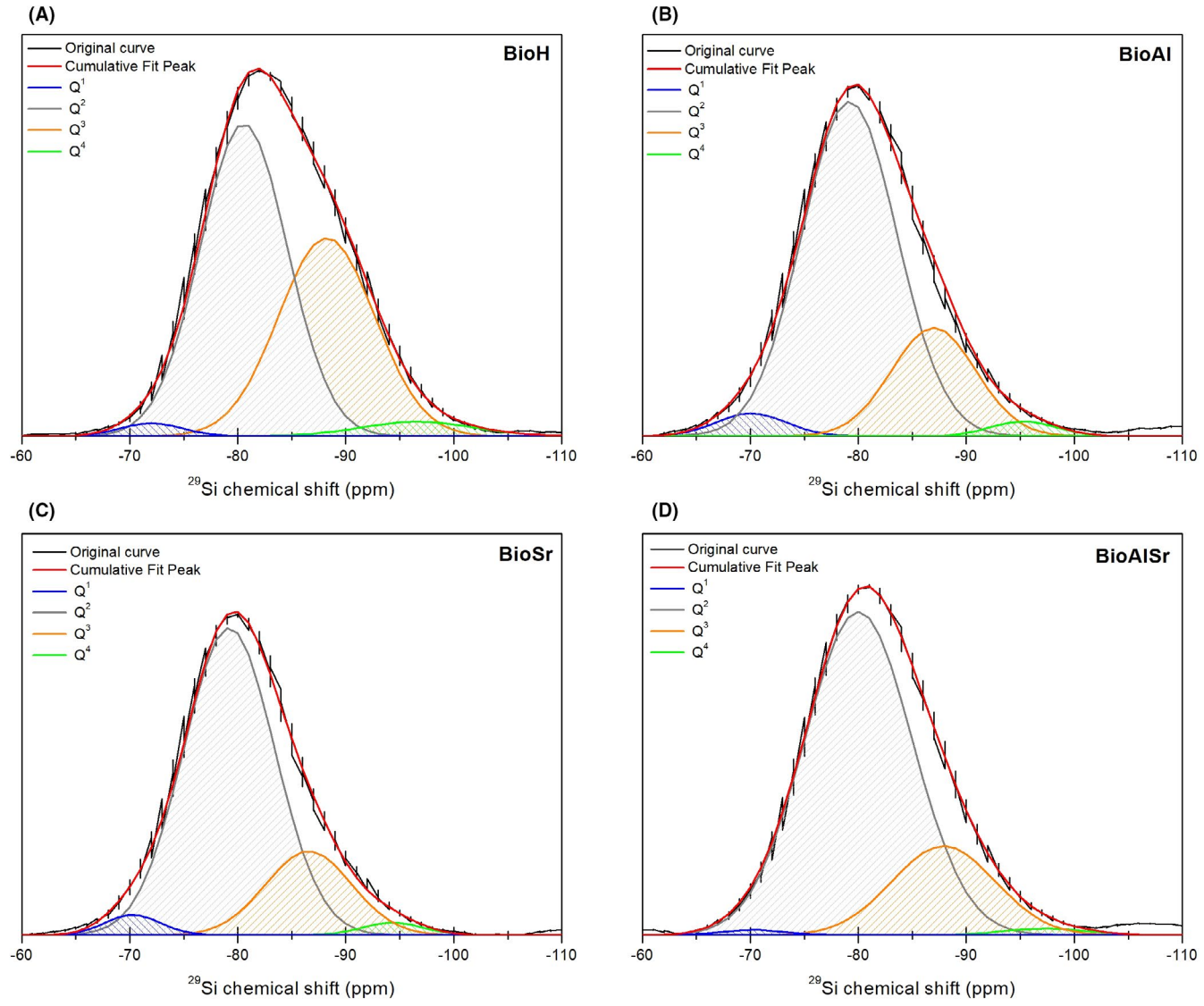

FIGURE 4 Deconvolution of 29Si MAS-NMR spectra for bioactive glasses. MAS-NMR, magic angle spinning nuclear magnetic resonance [Color figure can be viewed at wileyonlinelibrary.com]

TABLE 3 ^{29}Si MAS-NMR parameters of the bioactive glasses: Q^n distribution by peak deconvolution and % calculated from the fractional areas

	Q^1		Q^2		Q^3		Q^4	
Sample	**Center (ppm)**	**%Area**	**Center (ppm)**	**%Area**	**Center (ppm)**	**%Area**	**Center (ppm)**	**%Area**
BioH	−70.98	1.63	−80.55	55.85	−88.23	39.20	−96.64	3.31
BioAl	−70.07	3.65	−79.18	73.08	−87.98	21.05	−96.28	2.21
BioSr	−70.29	2.91	−80.01	76.53	−87.57	18.59	−96.34	1.97
BioAlSr	−70.22	0.75	−80.01	77.49	−87.90	20.50	−97.37	1.25

Abbreviation: MAS-NMR, magic angle spinning nuclear magnetic resonance.

one asymmetric broad component centered at −8.4 ppm. However, BioSr spectra presented a slight displacement toward positive values centered at −5.9 ppm. Despite this change, no significant differences were detected suggesting that most sodium ions occupy similar environments.

Figure 5C shows ^{27}Al MAS-NMR spectra of glasses BioAl and BioAlSr indicates that aluminum atoms were successfully integrated into silicate network by presenting a resonance centered at 59.5 ppm characteristic of the four-coordinated form ($Al(OSi)_4^-$), whose negative charge

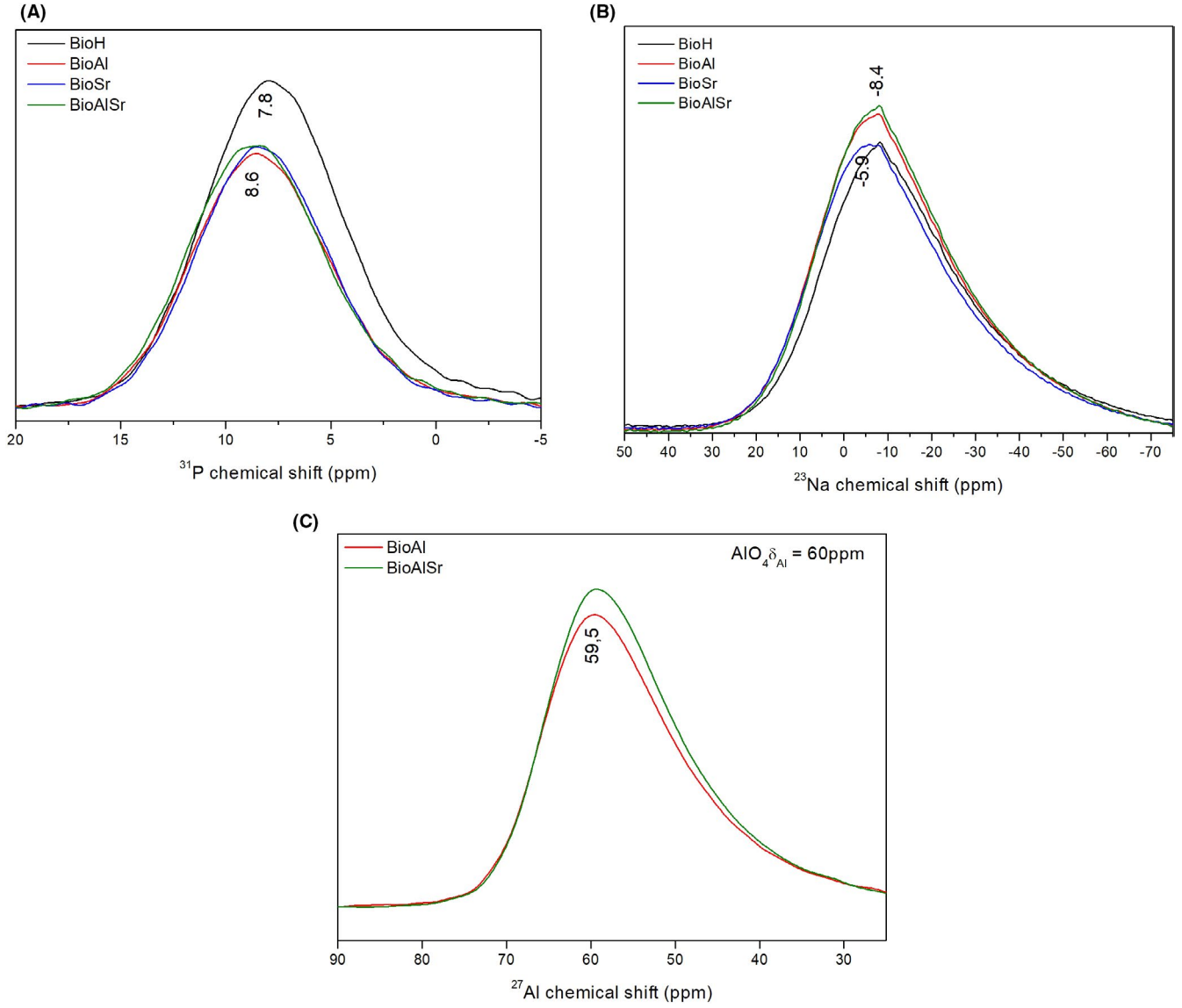

FIGURE 5 MAS-NMR spectra of (A) 31P, (B) 23Na and (C) 27Al for bioactive glasses. MAS-NMR, magic angle spinning nuclear magnetic resonance [Color figure can be viewed at wileyonlinelibrary.com]

is charge balanced by Ca^{2+} ions. The results are in accordance with the displacement found in ^{31}P NMR spectra where a favoring of sodium orthophosphate environment was observed in detriment of a smaller quantity of Ca^{2+} available.

Apart from NMR, Raman spectroscopy is a complementary tool to determine the structure, environment, and dynamics of glassy materials. Also, it was the only technique for this purpose performed in bulk instead of powder sample, ie on the surface of the obtained material. In silicate glass, the most interesting bands were associated with vibrations of asymmetric and symmetric stretching are in the region between 800 and 1200 cm^{-1}. For either spectroscopy and deconvolution set up was an adopted method created by Mysen et al and Brow.[43,44] For better fitting (the correlation coefficient $R^2 > .998$) was assumed the presence not only of $Q_{Si}{}^2$, $Q_{Si}{}^3$ but $Q_{Si}{}^0$ and $Q_{Si}{}^1$ as well. So, the attributions considered for the fitting were as follows:

1. 864 cm^{-1} of Q^0 units;
2. 906 cm^{-1} of Q^1 units;
3. 944 cm^{-1} of Q^2 units;
4. 974 cm^{-1} for P-O-P stretching;
5. 1008 cm^{-1} ^{0}O-P-O$^-$ stretching of P_2O_5 sheet unit;
6. 1044 cm^{-1} asymmetric stretching of bridge oxygen (BO) in all Q species;
7. 1086 cm^{-1} symmetric stretching of Q^3 units.

Agreeing with NMR results, all samples presented a high intensity for $Q_{Si}{}^2$ units. No significant changes were observed in respect of Q species however, P bands were very sensitive to this analysis (Figure 6, Table 4). Although P units are present in

the network as orthophosphate in BioSr was observed a bigger loss from the contribution at 1008 cm^{-1} corresponded to ^{0}O-P-O^{-} stretching of P_2O_5 sheet unit to a direct gain at 1044 cm^{1} characteristic of asymmetric stretching of BO in all *Q* species. It seems that the incorporation of strontium does not cause a considerable change in the local sphere but in a mid-range scale, its presence influences the arrangement of P in the glass network. It is known the role of P in the bioactive glasses and that its specific amount triggers the phase separation in this kind of multi component glass.[45] Also, many studies were taken into account the probability of network modifiers cluster, such as Na, Ca, and Sr especially if there are small changes in the alkali ratio (Na:Ca/Sr) which do not alter network connectivity but changes will be reflected at most of the chemical and physical glass properties. Likewise, it was found that phosphorous and Ca/Sr ions are preferentially clustered.[46,47] It can be stated that the presence of an excess of strontium has favored glass in glass separation clustering with phosphorus instead of being in a linear sheet subnetwork with phosphorus as expected and observed in the other samples. To be representative, each sample was three times evaluated by changing the zone of measurement, in the samples BioH, BioAl and BioAlSr, all spectra were similar, unlike BioSr which all spectra (not presented in this article) was distinct, supporting the clustering theory.

Finally, the increase in stretching asymmetric BO in silicon tetrahedral could be due to a change in the Q_{Si}^{2} units. As previous mentioned, Q_{Si}^{2} in a suchlike composition can occur in chains and/or ring units and their occurrence is directly connected with their number and coordination of oxygen. Usually, there is no difference observed at a chemical shift in NMR analysis, but it can be evaluated from the crystalline phase raised from the thermal temperature at adequate temperatures. As observed from the diffractogram of treated samples, a different phase of combeite was formed in BioSr. According to Volzone and Stábile[27] both high and low combeite would be formed by similar composition and depends on sodium and calcium content in the phosphorous environment. Still, they observed that higher sodium content with phosphorous originated greater relative amount of high combeite ($Na_2CaSi_2O_6$).

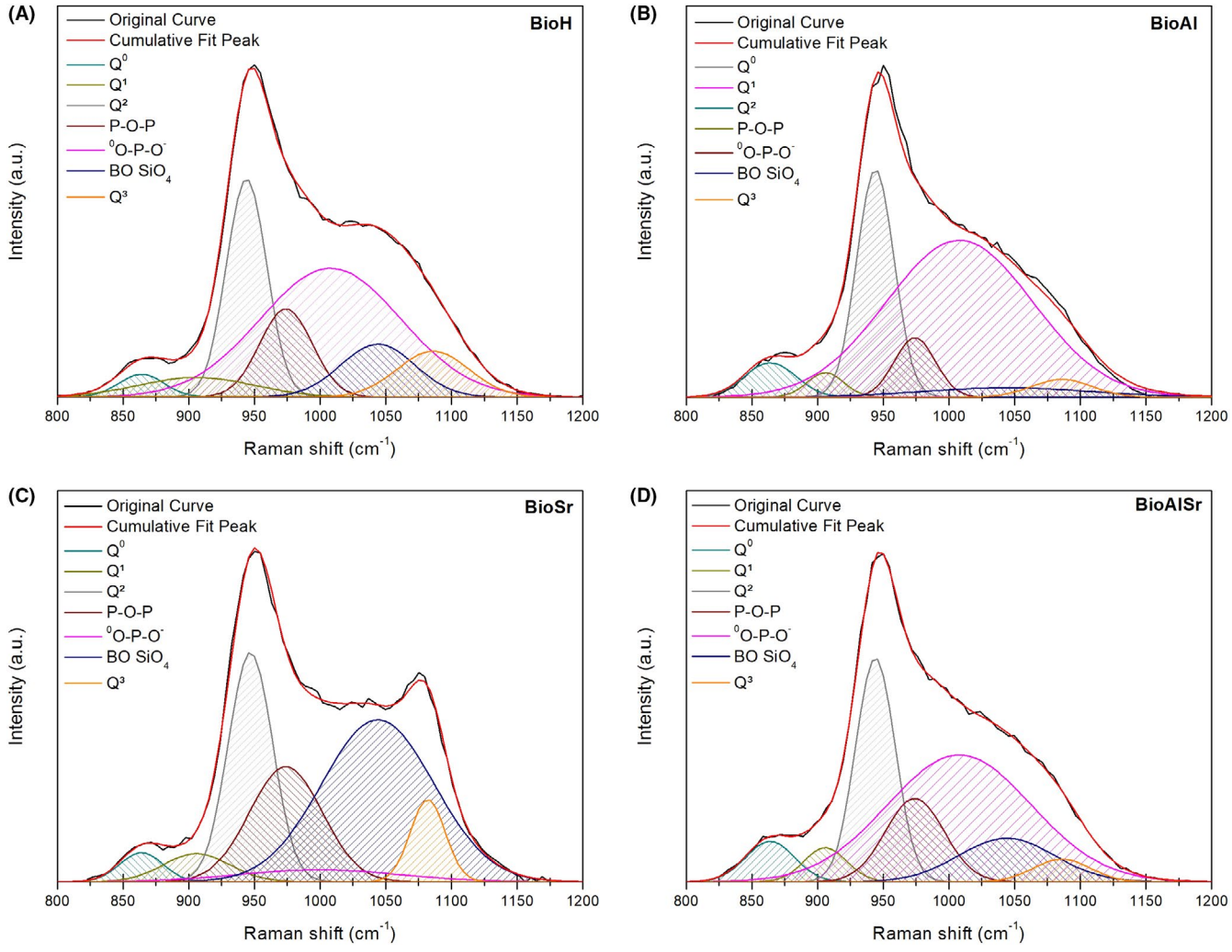

FIGURE 6 Deconvolution of Raman spectra for untreated bioactive glasses [Color figure can be viewed at wileyonlinelibrary.com]

TABLE 4 Frequency and percentage for Raman bands of the bioactive glasses

Sample	$\%Q^0$, 864	$\%Q^1$/O-O, 906	$\%Q^2$, 944	%P-O-P, 974	$\%^0$O-P-O$^-$, 1008	%BO SiO_4, 1044	$\%Q^3$, 1086
BioH	2.44	5.31	20.95	11.02	43.12	9.32	7.84
BioAl	4.48	2.28	21.67	6.21	58.70	3.95	2.72
BioSr	2.81	4.18	22.78	18.76	4.26	40.77	6.46
BioAlSr	4.83	3.55	21.65	11.96	44.73	10.16	3.14

Abbreviation: BO, bridging oxygen.

Further investigations will focus on how the changes in compositions selected in this study affect mechanical and tribological behavior as well as in vitro biological and morphological evaluation. Optimistically, this should lead toward a material with enhanced performance not only in processing but also in lower brittleness without compromise the beneficial ability to dissolve and bond to bone-like 45S5.

4 | CONCLUSIONS

A new modified composition of bioactive glass was presented. The use of small quantities of oxides is potentialized by the presence of a secondary vitreous former. The results revealed that the incorporation of Al_2O_3 as a four-coordinated form was essential for optimize the influence of SrO in the system. The tendency of 2 mol% of strontium oxide to trigger its segregation into clusters was inhibited with the presence of Al_2O_3. Despite Q^n distribution was predominantly Q^2 in all samples, the composition criteria used caused a rearrangement of silica network impacting principally thermal properties enabling improved processing and stability characteristics. The addition of Al_2O_3 and SrO into BioAlSr promoted a larger sinterability parameter which indicates better sintering behavior, the glass stability against crystallization doubled compared to 45S5 (BioH) and the processing window enlarged from 106 to 171. Also, developed BioAlSr revealed to maintain the formation of combeite type of crystalline phase after heat treatment at 800°C for 2 hours. The findings in this study outperform a poor processing window and a high tendency to crystallization of Bioglass® 45S5 apart from highlighting important differences in ways of interaction of 2 mol% of strontium in 45S5 and in a composition where a small amount of alumina acts partially as former oxide.

ACKNOWLEDGMENTS

This research was performed with support from the Brazilian government through their respective funding agencies CAPES (CsF/PDSE-Project No 88881.189953/2018-01), CNPq (GD-Project No 142172/2016-2), and FAPESP (Project No 2000/02483-9).

ORCID

Mariana S. Araujo https://orcid.org/0000-0002-0519-6263
José F. Bartolomé https://orcid.org/0000-0002-7515-4202

REFERENCES

1. Boccaccini AR, Chen Q, Lefebvre L, Gremillard L, Chevalier J. Sintering, crystallisation and biodegradation behaviour of Bioglass®-derived glass-ceramics. Faraday Discuss. 2007;136:27–44.
2. Groh D, Döhler F, Brauer DS. Bioactive glasses with improved processing. Part 1. Thermal properties, ion release and apatite formation. Acta Biomater. 2014;4465–73.
3. Kargozar S, Montazerian M, Fiume E, Baino F. Multiple and promising applications of strontium (Sr)-containing bioactive glasses in bone tissue engineering. Front Bioeng Biotechnol. 2019;7:161.
4. Kaur G, Kumar V, Baino F, et al. Mechanical properties of bioactive glasses, ceramics, glass-ceramics and composites: state-of-the-art review and future challenges. Mater Sci Eng C. 2019;104:109895.
5. Hamilton JP, Pantano CG. Effects of glass structure on the corrosion behavior of sodium-aluminosilicate glasses. J Non Cryst Solids. 1997;222:167–74.
6. Hench LL, Roki N, Fenn MB. Bioactive glasses: importance of structure and properties in bone regeneration. J Mol Struct. 2014;1073:24–30.
7. Massera J, Hupa L. Influence of SrO substitution for CaO on the properties of bioactive glass S53P4. J Mater Sci Mater Med. 2014;25:657–68.
8. Hill RG, Brauer DS. Predicting the glass transition temperature of bioactive glasses from their molecular chemical composition. Acta Biomater. 2011;7:3601–5.
9. Rabiee SM, Nazparvar N, Azizian M, Vashaee D, Tayebi L. Effect of ion substitution on properties of bioactive glasses: a review. Ceram Int. 2015;41:7241–51.
10. Kargozar S, Baino F, Hamzehlou S, Hill RG, Mozafari M. Bioactive glasses entering the mainstream. Drug Discovery Today. 2018;23:1700–4.
11. Moghanian A, Firoozi S, Tahriri M, Sedghi A. A comparative study on the in vitro formation of hydroxyapatite, cytotoxicity and antibacterial activity of 58S bioactive glass substituted by Li and Sr. Mater Sci Eng C. 2018;91:349–60.
12. Arepalli SK, Tripathi H, Hira SK, Manna PP, Pyare R, Singh SP. Enhanced bioactivity, biocompatibility and mechanical behavior of strontium substituted bioactive glasses. Mater Sci Eng C. 2016;69:108–16.
13. Christie JK, de Leeuw NH. Effect of strontium inclusion on the bioactivity of phosphate-based glasses. J Mater Sci. 2017;52:9014–22.
14. Oryan A, Eslaminejad MB, Kamali A, Hosseini S, Sayahpour FA, Baharvand H. Synergistic effect of strontium, bioactive glass and

nano-hydroxyapatite promotes bone regeneration of critical-sized radial bone defects. J Biomed Mater Res B Appl Biomater. 2018;107:50–64.
15. Marie PJ. Strontium as therapy for osteoporosis. Curr Opin Pharmacol. 2005;5:633–6.
16. Tripathi H, Rath C, Sampath A, Pratim P. Structural, physico-mechanical and in-vitro bioactivity studies on SiO_2-CaO-P_2O_5-SrO-Al_2O_3 bioactive glasses. Mater Sci Eng C. 2019;94:279–90.
17. Liu H, Yang R, Wang Y, Liu S. Influence of alumina additions on the physical and chemical properties of lithium-iron-phosphate glasses. Phys Procedia. 2013;48:17–22.
18. Da Silva AC. Structure and percolation of bioglasses. In: Marchi J, editor. Biocompatible glasses. Cham, Switzerland: Springer, 2016; p. 49–84.
19. Du J, Xiang Y. Effect of strontium substitution on the structure, ionic diffusion and dynamic properties of 45S5 bioactive glasses. J Non Cryst Solids. 2012;358:1059–71.
20. Moya JS, Cabal B, Sanz J, et al. Mechanism of calcium lixiviation in soda-lime glasses with a strong biocide activity. Mater Lett. 2012;70:113–5.
21. Esteban-Tejeda L, da Silva AC, Mello-Castanho SR, Pecharromán C, Moya JS. Kinetics of dissolution of a biocide soda-lime glass powder containing silver nanoparticles. J Nanopart Res. 2013;15:1447.
22. Moya JS, Esteban-Tejeda L, Pecharromán C, Mello-Castanho SR, Da Silva AC, Malpartida F. Glass powders with a high content of calcium oxide: a step towards a "green" universal biocide. Adv Biomater. 2011;13:256–60.
23. Baino F. Bioactive glasses – when glass science and technology meet regenerative. Ceram Int. 2018;44:14953–66.
24. Brauer DS, Brückner R, Tylkowski M, Hupa L. Sodium-free mixed alkali bioactive glasses. Biomed Glass. 2016;2:99–110.
25. Tylkowski M, Brauer DS. Mixed alkali effects in Bioglass® 45S5. J Non Cryst Solids. 2013;376:175–81.
26. Bellucci D, Cannillo V, Sola A. An overview of the effects of thermal processing on bioactive glasses. Sci Sinter. 2010;42:307–20.
27. Volzone C, Matías SF. Structural changes by thermal treatment up to glass obtention of P_2O_5-Na_2O-CaO-SiO_2 compounds with bioglass composition types. New J Glas Ceram. 2013;3:53–7.
28. Lefebvre L, Chevalier J, Gremillard L, et al. Structural transformations of bioactive glass 45S5 with thermal treatments. Acta Mater. 2007;55:3305–13.
29. Peitl O, Dutra Zanotto E, Hench LL. Highly bioactive P_2O_5–Na_2O–CaO–SiO_2 glass-ceramics. J Non Cryst Solids. 2001;292:115–26.
30. Daguano JKMF, Rogero SO, Crovace MC, Peitl O, Strecker K, Dos Santos C. Bioactivity and cytotoxicity of glass and glass-ceramics based on the 3CaO·P_2O_5-SiO_2-MgO system. J Mater Sci Mater Med. 2013;24:2171–80.
31. Lara C, Pascual MJ, Durán A. Glass-forming ability, sinterability and thermal properties in the systems RO–BaO–SiO_2 (R=Mg, Zn). J Non Cryst Solids. 2004;348:149–55.
32. Kapoor S, Brazete D, Pereira IC, et al. Impact of transition metal ions on the structure and bioactivity of alkali-free bioactive glasses. J Non Cryst Solids. 2019;506:98–108.
33. Chen X, Chen X, Brauer DS, et al. Sodium is not essential for high bioactivity of glasses. Int J Appl Glass Sci. 2017;8:428–37.
34. Fujikura K, Karpukhina N, Kasuga T, Brauer DS, Hill RG, Law RV. Influence of strontium substitution on structure and crystallisation of Bioglass® 45S5. J Mater Chem. 2012;22:7395.
35. Bellucci D, Cannillo V. A novel bioactive glass containing strontium and magnesium with ultra-high crystallization temperature. Mater Lett. 2018;213:67–70.
36. Brow RK. Nature of alumina in phosphate glass: I, properties of sodium aluminophosphate glass. J Am Ceram Soc. 1993;76:913–8.
37. Kapoor S, Semitela Â, Goel A, et al. Understanding the composition-structure-bioactivity relationships in diopside (CaO·MgO·2SiO_2)-tricalcium phosphate (3CaO·P_2O_5) glass system. Acta Biomater. 2015;15:210–26.
38. Eckert H. Structural characterization of bioactive glasses by solid state NMR. J Sol-Gel Sci Technol. 2018;88:263–95.
39. Edén M. NMR studies of oxide-based glasses. Annu Rep Sect "C" Phys Chem. 2012;108:177.
40. Martin RA, Twyman HL, Rees GJ, et al. A structural investigation of the alkali metal site distribution within bioactive glass using neutron diffraction and multinuclear solid state NMR. Phys Chem Chem Phys. 2012;14:12105.
41. Brow RK, Kirkpatrick RJ, Turner GL. Nature of alumina in phosphate glass: II, structure of sodium alurninophosphate glass. J Am Ceram Soc. 1993;76:919–28.
42. O'Donnell MD, Watts SJ, Law RV, Hill RG. Effect of P_2O_5 content in two series of soda lime phosphosilicate glasses on structure and properties – part II: physical properties. J Non-Cryst Solids. 2008;354(30):3561–6.
43. Brow RK. Review: the structure of simple phosphate glasses. J Non Cryst Solids. 2000;263-264:1–28.
44. Mysen BO, Ryerson FJ, Virgo D. The structural role of phosphorus in silicate melts. Am Mineral. 1981;66:106–17.
45. Tilocca A, Cormack AN. Structural effects of phosphorus inclusion in bioactive silicate glasses. J Phys Chem B. 2007;111:14256–64.
46. Xiang Y, Du J. Effect of strontium substitution on the structure of 45S5 bioglasses. Chem Mater. 2011;23:2703–17.
47. Christie JK, Ainsworth RI, de Leeuw NH. Investigating structural features which control the dissolution of bioactive phosphate glasses: Beyond the network connectivity. J Non Cryst Solids. 2016;432:31–4.

How to cite this article: Araujo MS, Silva AC, Bartolomé JF, Mello-Castanho S. Structural and thermal behavior of 45S5 Bioglass®-based compositions containing alumina and strontium. *J Am Ceram Soc*. 2020;103:3620–3630. https://doi.org/10.1111/jace.17061